Materials Science and Engineering A 551 (2012) 73–81

Contents lists available at SciVerse ScienceDirect

Materials Science and Engineering A

journal homepage: www.elsevier.com/locate/msea

Microstructure–hardness relationship in the fusion zone of TRIP steel welds

S.S. Nayak[a,*], V.H. Baltazar Hernandez[a,b], Y. Okita[a,c], Y. Zhou[a]

[a] Center for Advanced Materials Joining, Mechanical and Mechatronics Engineering, University of Waterloo, Waterloo, ON N2L 3G1, Canada
[b] MPyM-EPMM Academic Unit of Engineering, Autonomous University of Zacatecas, C.P. 98000 Zacatecas, Mexico
[c] Joining & Strength Research Department, JFE Steel Corporation, Chiba 260-0835, Japan

ARTICLE INFO

Article history:
Received 25 November 2011
Received in revised form 27 April 2012
Accepted 29 April 2012
Available online 8 May 2012

Keywords:
Transformation induced plasticity (TRIP) steel
Microstructure
Hardness
Resistance spot welding

ABSTRACT

Fusion zone of three TRIP steels, categorized as AT: C–Mn–Al, AST: C–Mn–Al–Si and ST: C–Mn–Si, in resistance spot welding was characterized with respect to microstructure, phase analysis, and hardness. The fusion zone microstructure was found to depend on chemistry: (i) AT steel contained ferrite phase surrounded by bainite and martensite regions, (ii) AST steel showed a bainite structures along with martensite laths and interlath retained austenite, whereas (iii) ST steel constituted single phase martensite laths with interlath austenite. X-ray diffraction study indicated that retained austenite fraction in the fusion zone increases with increase in Si content in it. The AST fusion zone hardness lies between those of the AT and ST steels; the ST fusion zone hardness was higher than that of AT steel because of the single phase martensite microstructure. Comparison of fusion zone microstructure and hardness to earlier study on laser welding of the TRIP steels with similar chemistries revealed that higher cooling rate in resistance spot welding led to higher fusion zone hardness compared to laser welding; which was attributed either to decrease in softer ferrite phase (AT steel) in the microstructure or refinement of martensite laths (ST steel).

1. Introduction

Automobile industries demand lightweight materials without compromising the strength. Many materials have been competing in the race to accomplish the requirement of automotive industries but advanced high strength steels (AHSS) have been the winner. Because, AHSS reduce the vehicle weight leading to reduced fuel consumption and increase the passenger safety due to higher energy absorption and stiffness of the body. AHSS is commonly referred to dual phase (DP), transformation induced plasticity (TRIP), complex phase (CP), and martensitic (M) steels which are characterized as steels with a yield strength above 300 MPa and a tensile strength higher than 600 MPa [1,2]. Among all the AHSS, TRIP steels have high strength combined with good uniform elongation due to hard–soft composite structure given by its various structural constituents like ferrite, bainite, martensite and carbon-enriched retained austenite [3–6]. TRIP steel is commonly alloyed with, apart from Mn, Si or Al to suppress cementite formation thus forcing more carbon into retained austenite as both Si and Al are insoluble in cementite [1,2]. The mechanical properties of the TRIP steels have been the special attention for the possible implementation in industries. No difference in mechanical properties of TRIP steels is observed when all the Si in it is replaced by Al [7]; but interestingly C–Mn–Al TRIP steel exhibits a remarkable TRIP effect during tensile testing compared to C–Mn–Si TRIP [8]. In this regard, TRIP steel alloyed with both Si and Al are being considered based on concept of partial replacement of Si by limited amount of Al [9].

Automotive industries adopt various welding techniques to join steel sheets for the assembly of car bodies and various structural components [10–18]. However, resistance spot welding (RSW) is currently one of the dominant methods for manufacturing auto-body structure [10,11,17,19–22]. In welding research, studies on welding of TRIP steels have been reported earlier by different processes [11–18]. For example, in laser beam welding (LBW) C–Mn–Si TRIP revealed a single phase martensite microstructure in the fusion zone [12–14]; whereas C–Mn–Al fusion zone formed a multiphase microstructure containing skeletal ferrite, bainitic ferrite, martensite and retained austenite [14–16]. Like in laser welding, C–Mn–Si fusion zone in RSW also formed single phase microstructure of martensite [11,17]. Although there are reports on evolution of fusion zone microstructure in C–Mn–Al TRIP and C–Mn–Si steel in different welding processes, there is lack of report on combined effect of Al and Si on the metallurgical and mechanical properties of the fusion zone in TRIP steel in RSW or any other welding

* Corresponding author. Tel.: +1 519 888 4567x35256; fax: +1 519 885 5862.
E-mail addresses: sashank@uwaterloo.ca, sashank.nayak@gmail.com (S.S. Nayak).

0921-5093/$ – see front matter © 2012 Elsevier B.V. All rights reserved.
http://dx.doi.org/10.1016/j.msea.2012.04.096

Table 1
Chemical composition of the studied steels in wt.% along with the M_s temperature (°C).

Steel	C	Mn	Si	Al	[a]M_s
AT	0.12	2.13	0.08	1.27	420
AST	0.16	1.9	0.85	0.65	415
ST	0.19	1.63	1.62	0.03	409

[a] M_s was calculated using equations reported earlier [14]. AT: C–Mn–Al, AST: C–Mn–Al–Si and ST: C–Mn–Si TRIP steel.

processes. Furthermore, higher cooling rate implemented by RSW compared to other welding processes at the fusion zone makes it an interesting process to explore.

The present study was focused on studying the microstructure and hardness of the fusion zone in RSW of TRIP steels. Fusion zone microstructure and hardness was compared based on three different chemistries of TRIP steel: C–Mn–Al, C–Mn–Al–Si, and C–Mn–Si. A detailed microstructural study was carried out mainly by transmission electron microscopy (TEM) along with scanning electron microscopy (SEM). The hardness results were compared by correlating to the corresponding fusion zone microstructure. In addition, the results of the present study were compared with the fusion zone in LBW of TRIP steels with similar chemistries.

2. Experimental details

The starting materials in this study were cold rolled (1.0 mm thickness) TRIP steels (UTS = 780 MPa). The denotation of the different TRIP steels, their chemistries and the martensite start (M_s) temperature are tabulated in Table 1. The M_s temperature was calculated using equations reported earlier [23]. The base metal microstructure of AT and ST steels is illustrated in Fig. 1 and their mechanical properties are listed in Table 2. It is to be noted that chemistry of the AST (C–Mn–Al–Si) steel is referred to the chemistry of the fusion zone developed in lap welding of AT and ST steel sheets. Thus, the chemistry of the AST steel was calculated by taking average of the chemistry of the AT and ST steels considering that liquefaction and mixing occurs during spot welding and also because both steel sheets are of similar thickness (1.0 mm). The equilibrium phase diagrams of the steels were calculated using commercial thermodynamic software (ThermoCalc Software AB, Stockholm, Sweden).

The TRIP steel sheets were joined by resistance spot welding (RSW) using a pneumatically controlled machine operated with an alternating current with frequency of 60 Hz. The parameters used in RSW process are given in Table 3. Electrode used in RSW was a truncated RWMA class 2 type with 6 mm face diameter [24]. A constant flow of water (4 l/min) was maintained for cooling the electrodes. All welding was carried out according to the American Welding Society recommended practice [25], the details of which are reported elsewhere [11]. The weld nugget size given in Table 3 was evaluated by metallographic sample preparation techniques. Sufficiently wide samples were sectioned across the weldment, covering all the weld zones i.e. fusion zone and heat affected zone (HAZ) along with the base metal. The specimens were mounted, grounded and polished followed by etching with Vilella's solution [26] for 6–8 s in order to delineate the weld nugget boundary (i.e. the fusion line). Minimum of four specimens were analyzed for measuring the width of the nugget and average values are presented. The cooling rate within the fusion zone was estimated from the temperature profile of the fusion zone (Fig. 2) obtained through numerical simulation using a commercial finite element software coupled with electrical–thermal–mechanical analysis, Quick Spot by Research Center of Computational Mechanics, Inc., Japan, was used to run the thermal simulation [27]. The details of the simulation procedure are reported in authors' previous work [28].

Table 2
Mechanical properties of the TRIP steels used in the study.

Code	YS (MPa)	UTS (MPa)	El. (%)	Hardness (HV)
AT	548	746	25	253 ± 13
ST	570	835	29	281 ± 12

YS: yield strength, UTS: ultimate tensile strength, and El.: elongation.

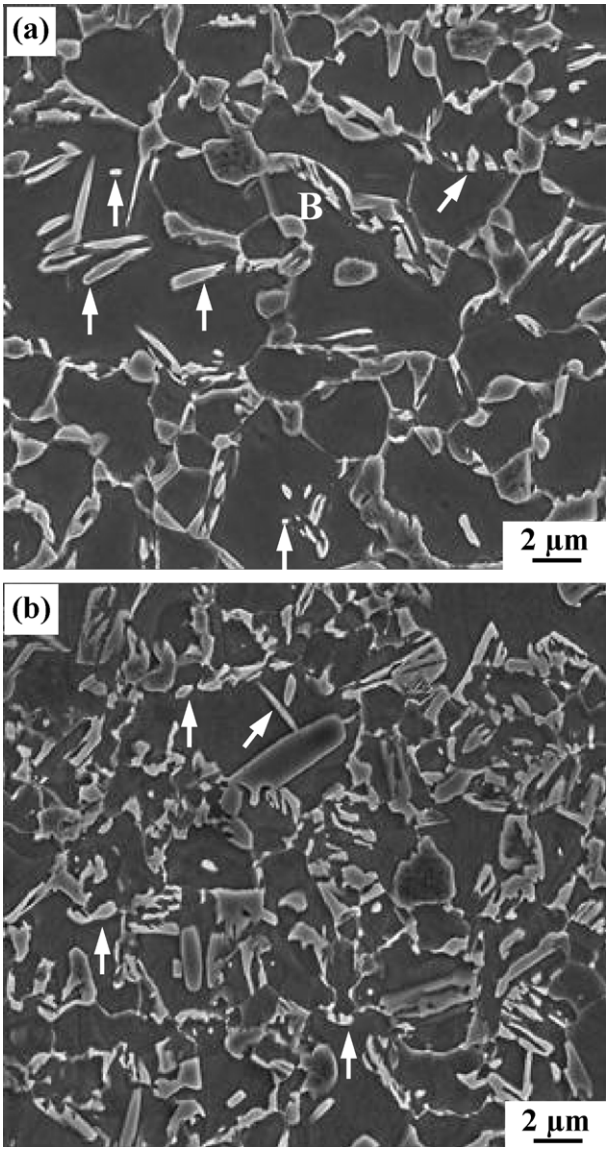

Fig. 1. Representative SEM micrographs illustrating as received (base metal) microstructures of: (a) AT steel and (b) ST steel. White arrows and letter B indicate untransformed austenite and bainite, respectively.

To examine the microstructure of different weld zones viz. fusion zone, HAZ and base metal by SEM, weld cross-sections were mounted in bakelite and mechanically polished using a series of SiC papers (320, 600, 800 and 1200 coarse, and 1200 fine), followed by mirror finished polishing using diamond suspensions (1 μm and 0.25 μm). The mirror finished samples were etched with 2% nital solution for examination of microstructure. A JEOL JSM 6460 scanning electron microscope was used for the investigation. Fraction of ferrite in the fusion zone was measured from at least ten SEM micrographs. Phase analysis of the FZ was done by X-ray diffraction (XRD) study carried out in a PHILIPS X'Pert diffractometer using Cu K_α radiation (λ = 1.5402 Å). Square sections containing the whole

Table 3
RSW parameters used to join the TRIP steels and the resulting nugget size of the welds.

Welding current (kA)	Force (kN)	Squeeze time (cycles)	Weld time (cycles)	Hold time (cycles)	Nugget size (mm)		
					AT	AST	ST
8	4.5	25	20	5	5.83	5.77	5.61

weld nugget were cut from the welds followed by mechanically grinding and polishing for the XRD study. TEM was employed to investigate the microstructure of the fusion zones only. TEM samples were prepared by sectioning rectangular samples from the welded sheets containing the fusion zone of the weld and subsequently grinding them to make foils of ~60–70 μm thickness. The rectangular samples were flipped over repeatedly during the grinding procedure in order to get foils close to the center line of the nugget (fusion zone). After that 3 mm disks were punched from the fusion zone regions which were revealed by etching the ground foils with 2% nital solution. Subsequently, the punched disks were electropolished in an electrolytic solution of 10% perchloric acid in methanol maintaining the bath temperature at below -15 °C. TEM studies were conducted using a PHILIPS CM12 microscope operated at 120 kV.

Vickers microhardness measurements on the welds were carried out using 200 g load with 15 s dwelling time. Firstly, hardness profiles were measured starting from center of fusion zone and running toward the base metal. In the case of AST, hardness measurements were carried out on both AT and ST steel sides and the average fusion zone hardness is reported. In addition to hardness profiles, a 3×3 matrix of indentation at the center of the fusion zone was carried out and the average of the nine measurements is reported as fusion zone hardness. A distance of 200 μm was maintained between consecutive indentations to avoid their interference.

3. Results and discussion

Fig. 1 illustrates the microstructure of the base metal (as received) of TRIP steels used in the present study. The different constituents of the microstructure in both the steels were ferrite matrix (dark regions), islands of transformed austenite products e.g. martensite and bainite (bright regions), and embedded untransformed/retained austenite (marked by arrows). A close observation of the microstructures revealed that AT steel has higher fraction of ferrite and less of retained austenite (Fig. 1a); whereas

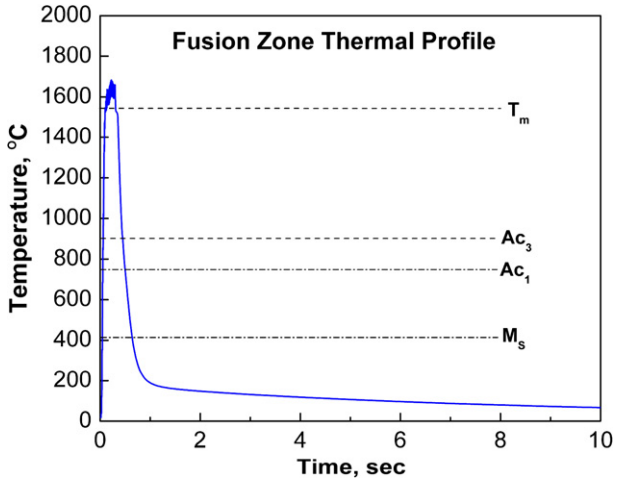

Fig. 2. Thermal profile of the fusion zone in RSW of TRIP steels investigated in the present study, taken from authors' earlier work [28].

lower fraction of ferrite in ST steel was compensated by increased untransformed austenite fraction (Fig. 1b) which is reported as the typical microstructure of Si-alloyed TRIP steel [2,14]. In addition, AT steel has higher fraction of bainite in the microstructure (marked as B in Fig. 1a), which is the result of Al-assisted accelerated bainitic transformation kinetics due to higher nucleation rate [29]. On the other hand alloying with Si retards the bainitic reaction in TRIP steel [2] thus negligible fraction of bainite was observed in it (Fig. 1b). Interestingly, the fraction of retained austenite is almost similar in the base metal microstructure of both the TRIP steels used in the present study which is achieved due to addition of Mn which is an austenite stabilizer [1].

3.1. Fusion zone microstructure of the TRIP steels

Representative SEM micrographs illustrating microstructure of the fusion zone of the steels are shown in Fig. 3. The AT steel fusion zone comprised a multiphase microstructure (Fig. 3a) containing martensite (bright regions) and significant amount ($15 \pm 3\%$) of skeletal ferrite (dark regions marked by F). AST fusion zone consisted of mixture of martensite and bainitic structure; whereas ST fusion zone microstructure was entirely single phase containing martensite (Fig. 3b). Similar results were also observed in laser beam welding (LBW) of similar TRIP steels studied by Xia et al. [14]; however, the volume fraction of skeletal ferrite was higher (30%) in the AT fusion zone. The lower fraction of skeletal ferrite in the current study is ascribed to higher cooling rate achieved by RSW in comparison to LBW [30], the details of which will be discussed in the sections following.

Interestingly, bright field TEM imaging indicated that microstructure of AT fusion zone essentially consists of ferrite surrounded by martensite (M) and upper bainite (UB) regions (Fig. 4a). In contrary, ST fusion zone revealed martensite laths and interlath austenite (marked by white arrows) as shown in Fig. 4b corroborating the SEM results (Fig. 3b). On the other hand, martensite laths were the main microstructural constituent in the fusion zone of the AST steel (Fig. 5). Different orientations of martensite laths were observed (Fig. 5a) along with occasional presence of finer martensite laths as shown in Fig. 5b. The martensite laths in the fusion zone contained interlath retained austenite films (dark lines) as illustrated in the bright field image (Fig. 5c). Inset in Fig. 5c is the selected area diffraction pattern of the corresponding region which was indexed to illustrate Kurdjumov–Sachs (K–S) orientation relationship i.e. $[-1\,1\,-1]_{\alpha'}//[-1\,1\,0]_{\gamma}$ between martensite lath and interlath retained austenite with body centered tetragonal and face centered cubic structure, respectively. It may be mentioned here that K–S orientation relationship is one of two most widely reported orientation relationships between austenite and martensite; other one being Nishiyama–Wasserman (N–W) [31]. The dark field image (Fig. 5d) taken using austenite $(-2\,2\,0)$ diffraction spot, of the region illustrated in Fig. 5c, confirmed the presence of retained austenite films at martensite interlath boundaries.

XRD patterns also confirmed the presence of retained austenite along with martensite/ferrite in the fusion zone microstructure as shown in Fig. 6. The peaks of bcc-martensite (α') and austenite (γ) were indexed in the XRD profile corroborating the microstructure observed in the fusion zone (Figs. 4 and 5). It may be noted that

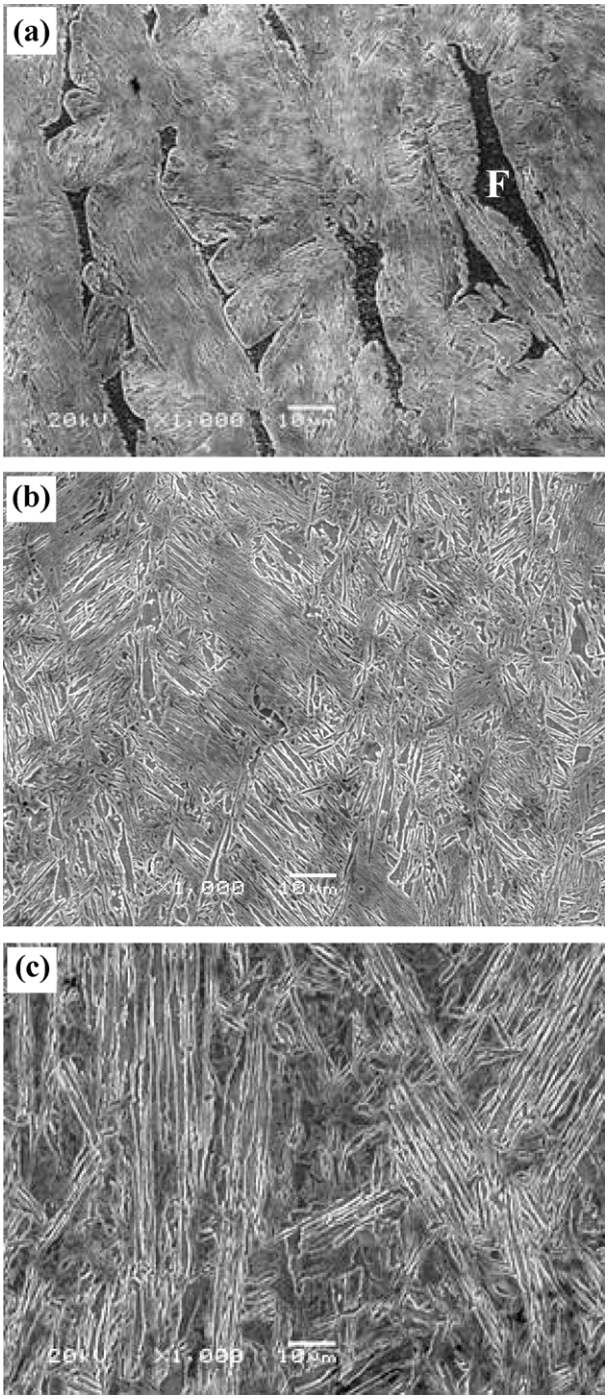

Fig. 3. Representative SEM micrographs illustrating fusion zone microstructure of: (a) AT steel containing ferrite in martensite and/or bainite matrix, (b) AST steel showing mixture of bainite and martensite, and (c) ST steel depicting formation of single phase martensite.

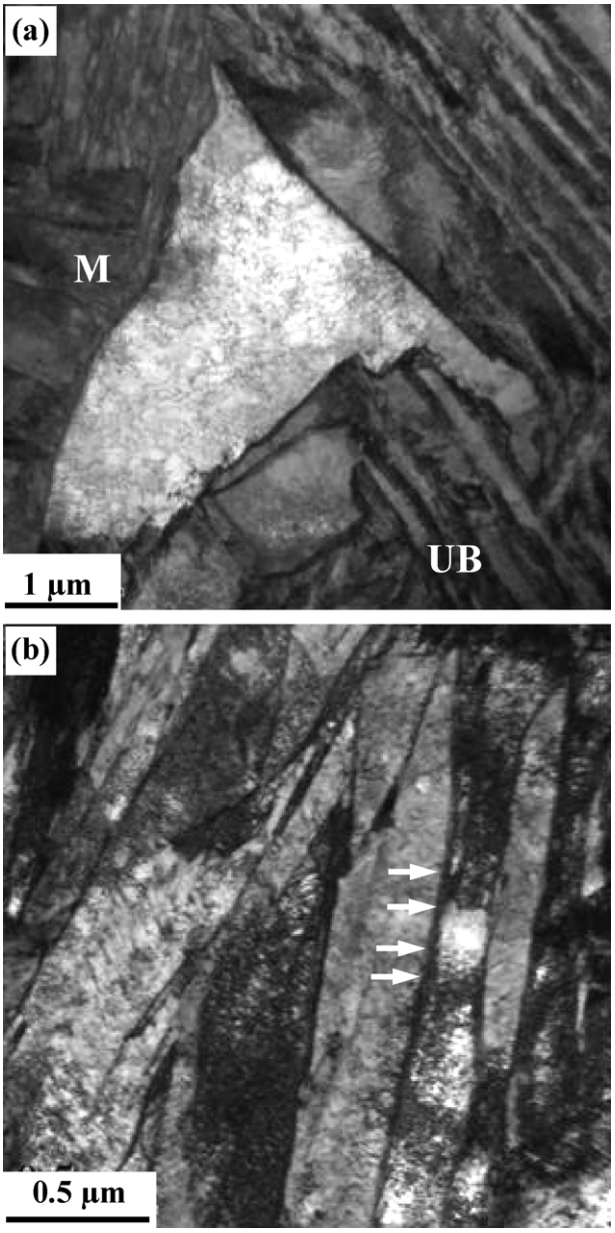

Fig. 4. Representative TEM images of fusion zone in the welds of: (a) AT steel showing a ferrite grain surrounded by martensite and upper bainite matrix phases, and (b) ST steel showing single phase microstructure containing martensite laths and interlath retained austenite (marked by white arrows). M: martensite, UB: upper bainite.

the diffraction peaks of martensite and ferrite overlaps so it is difficult of distinguish between the two from XRD peaks. However, it is clearly seen that the number and intensity of the austenite peaks is lowest in AST and highest in ST; whereas the AST has the intermediate value indicating that with increase in Si-content in the fusion zone the amount of interlath austenite formation increases in the trend AT(0.008Si) → AST(0.85Si) → ST steel(1.62Si); which also implies the increase in martensite laths in the microstructure.

Interestingly, apart from lathy martensite morphology AST fusion zone contained bainitic regions and occasional presence of martensite twins in the microstructure as delineated by the representative TEM micrographs (Fig. 7). The fraction of bainite in the AST fusion zone microstructure was measured from 10 bright field images to be 20%. The microstructure shown in Fig. 7a resembles well to typical lower bainite structure containing multiple variants of cementite precipitates within bainitic-ferrite laths [1,32]. Upper bainite formation was another aspect of the AST fusion zone microstructure (Fig. 7b) depicting unique features containing sheaves with fine plates (~0.2 μm thick) of bainitic-ferrite separated by cementite plates [1,32]. Additionally, there were regions with coexistence of both lower and upper bainite within the fusion zone (Fig. 7b). Dark field image (Fig. 7c), taken using $(-2\,1\,0)$ spot of θ-Fe_3C, confirms the presence of cementite plates in between bainitic-ferrite laths. The selected area diffraction pattern (inset in Fig. 7c) of the upper bainite region in Fig. 7b showed a

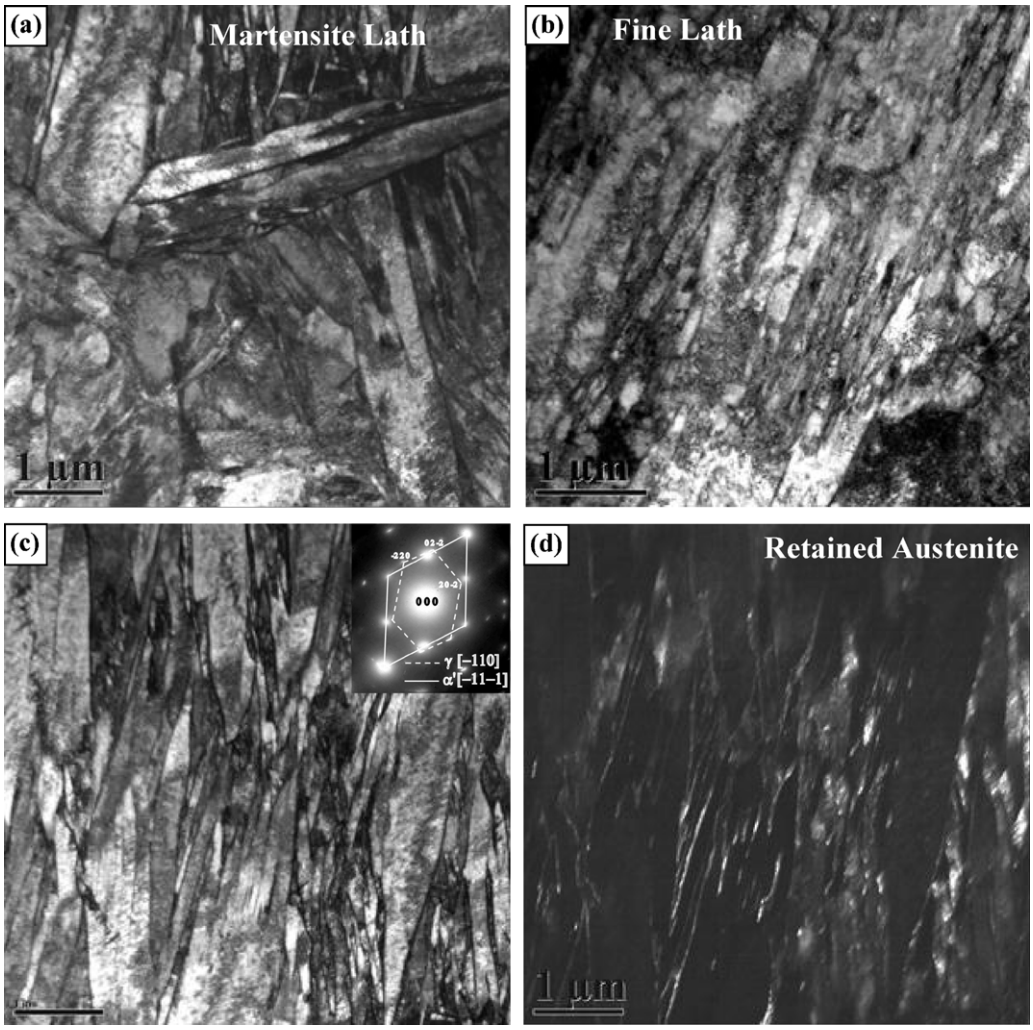

Fig. 5. Representative TEM images delineating martensite structure in the AST fusion zone: (a) martensite grains/packets, (b) finer laths, (c) martensite laths separated by retained austenite films, inset is the indexed diffraction pattern showing K–S relationship, and (d) dark field image taken using austenite (−2 2 0) confirming the retained austenite films in (c).

composite spot pattern demonstrating $[1\,1\,3]_{\alpha\text{-Fe}}//[1\,2\,-3]_{\theta\text{-Fe}_3\text{C}}$ orientation relationship between Fe_3C (orthorhombic) and α-Fe (body centered cubic) phases. Apart from bainite, occasional occurrence of martensite twins associated with high dislocation density

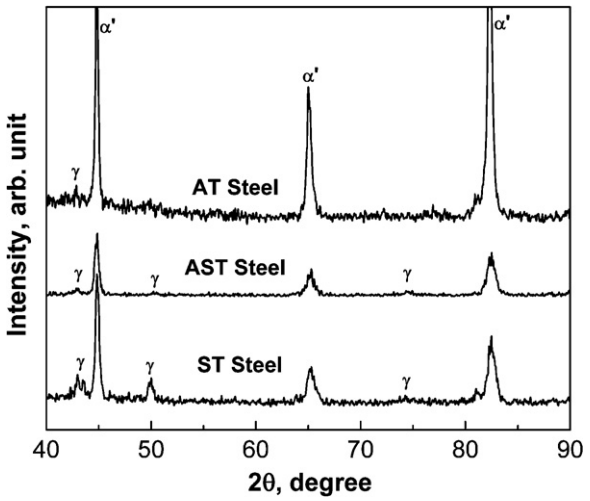

Fig. 6. XRD patterns of the fusion zone of TRIP steels illustrating formation of martensite (α′) and retained austenite (γ).

was observed in the mixed-TRIP fusion zone (Fig. 7d) similar to results reported on LBW of C–Mn–Al TRIP (AT) steel [15]. Formation of bainitic structure in the fusion zone is attributed to alloying the TRIP steel with Al that accelerates the kinetics of bainite formation by enhancing nucleation rate [29]. The present observation is corroborated well by earlier reports on formation of bainite in the fusion zone of Al-TRIP steel joined by LBW [14–16]. However, it may be noted that cementite plates observed in upper bainite regions in the present study were not observed in laser welding of Al-TRIP steel [15]. This is attributed to combined effort of higher Al (1.73 wt.%) content, compared to 0.65 wt.% in the AST fusion zone, which helps in austenite stabilization by preventing formation of carbides [1,2,32] and higher cooling rate in RSW which decreases the time allowed for the diffusion of elements into austenite during the process of bainitic reaction. With the above mentioned results on microstructural study, it was concluded that fusion zone microstructure of AST steel contains various features viz. lathy martensite with interlath retained austenite (Fig. 5), lower bainite (Fig. 7a), upper bainite with cementite plates (Fig. 7b and c) and occasional presence of martensite twins (Fig. 7d).

3.2. Martensite and retained austenite formation

The microstructure forming in the fusion zone depends on two factors: cooling rate and chemical composition. In the present

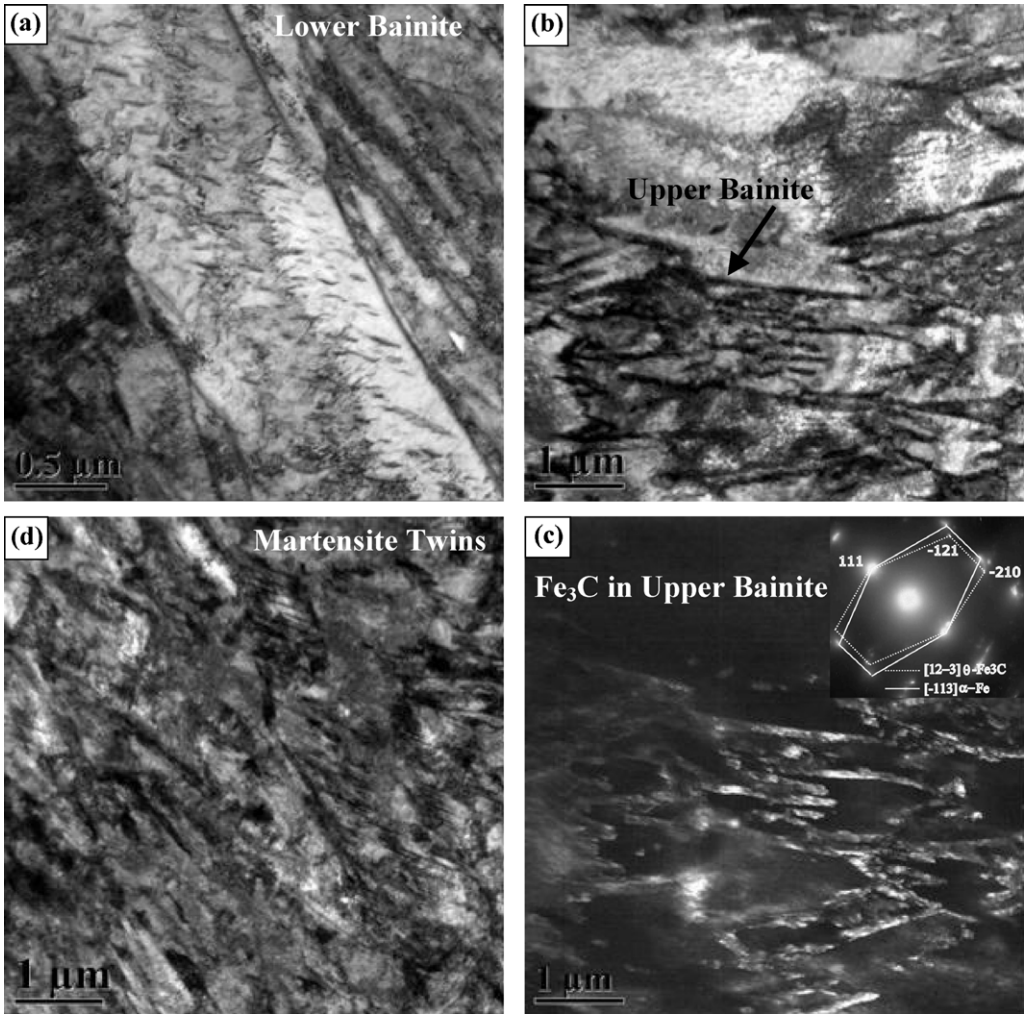

Fig. 7. Microstructure of AST steel fusion zone showing: (a) lower bainite, (b) bainitic ferrite laths (bright region) with interlath cementite plates (dark areas), (c) dark field image of (b) taken using θ-Fe_3C (−2 1 0) spot confirming the cementite plates. The inset in (c) depicts the indexed composite spot patterns of upper bainite region (marked by black arrow) showing $[1\ 2\ -3]_{\theta\text{-}Fe_3C}//[1\ 1\ 3]_{\alpha\text{-}Fe}$ orientation relationship, (d) martensite twins.

study, the cooling rate was estimated by simulation to be similar (>3000 K/s, Fig. 2) in all fusion zones considering the welding parameters were same for all welds; besides, materials type (TRIP780 steel) and thickness (1.0 mm). The simulated cooling rate in the fusion zone in the present study was in good agreement with that reported by Gould et al. [30]. The critical cooling rates for the formation of martensite for several AHSS when subjected to different welding techniques, such as RSW, LBW and resistance mesh seam welding (RMSEW) were reported recently [30]. In the report, the critical cooling rate for martensite formation for AHSS was estimated to be in the range 70–13,500 K/s depending on the steel chemistry. For TRIP800 steel, the critical cooling rate was calculated to be 90 K/s, which is well below the cooling rate attained in RSW i.e. >3000 K/s. Thus, in accordance to the cooling rate TRIP steels subjected to RSW should form single phase martensite phase in the fusion zone which is contrary to the observations in the present study as mentioned in foregoing paragraphs.

It is well known that Mn is added to increase the hardenability of TRIP steel so that martensite can form easily during fast cooling and quenching [1,2]. In the present study, due to high concentration of Mn (>1.6 wt.%) in all the TRIP steels (Table 1) martensite was the one of the primary microstructural constituents. However, high Mn content also results in excessive stabilization of retained austenite [1,2,33] which is manifested by the interlath austenite in the fusion zone microstructure (Figs. 4 and 5). In AT fusion zone ferrite was one of the major phases, the formation of which will be discussed in following section. Another reason for retained austenite in the fusion zone could be the carbon enrichment of austenite [1]. Similar observation of retained austenite at interlath boundaries was observed in the diode laser welds of TRIP steel of similar composition which was reported recently [14–16]. However, the reports that austenite is retained within bainitic-ferrite laths stabilized by sufficient Al-content (1.73 wt.%) during bainitic reaction [1,15]. Additionally, the chunk shaped austenite morphology observed in the fusion zone of laser welded Al-containing TRIP steel [14,15] was not observed in the present study. This can be attributed to the cooling rate in RSW (>3000 K/s) which is high enough to retard significant retained austenite stabilization by inhibiting carbon diffusion in comparison to cooling rate of 53 K/s in LBW [34]. In addition, mixing two different steels i.e. AT and ST, in the present study further diminished the chance of blocky retained austenite formation in AST fusion zone due to chemistry dilution. The above-mentioned discussion indicated that steel chemistry is the only

factor inducing the difference in the fusion zone microstructure constituents; the details of which are described in the following sections.

3.3. Ferrite stabilization and bainite formation in Al-containing steel

As per the observations of microstructure, skeletal ferrite was a major phase in the AT fusion zone (Figs. 3a and 4a) in contrast to AST and ST fusion zones wherein martensite was the dominating phase (Figs. 3b, c, 4b, and 5). It may be mentioned here that skeletal morphology is typical of high temperature δ-ferrite [14,18,35], thus ferrite observed in the present study was concluded to be δ-ferrite. The choice of Al or Si as alloying element in TRIP steel is important for retarding carbide precipitation and development of microstructures. Al-TRIP steel, as in the present study, is generally alloyed about 1–1.3 wt.% Al in order to suppress the formation of iron carbides and stabilize the austenite at room temperature [18,35]. According to Fe–Al binary phase diagram, if the Al content exceeds 1.05 wt.% than δ-ferrite is stabilized in the microstructure (Fig. 8a); whereas Si content has to be as high as 1.95 wt.% for δ-ferrite stabilization (Fig. 8b). Therefore, ferrite phase was not observed in the AST and ST fusion zones because of the lower Al-content i.e. 0.65 wt.% and 0.03 wt.%, respectively (Table 1); whereas sufficient Al content (1.27 wt.%) in AT steel facilitated δ-ferrite stabilization in the fusion zone (Figs. 3a and 4a).

Furthermore, Al is a strong ferrite stabilizer and promotes it as the primary phase in the microstructure [1,14,18,35]. For example, in welds made by striking an arc on a stationary Fe–0.23C–0.56Mn–0.26Si–1.77Al steel cylinder, ferrite with skeletal morphology (δ-ferrite) was stabilized at room temperature at a solidification cooling rate of as high as 10^3 K/s [35]. Furthermore, a study on microstructural evolution in Al-TRIP welded by gas tungsten arc welding indicated formation of δ-ferrite phase in the fusion zone and at fusion line [18]. Xia et al. [14] have also identified skeletal ferrite in LBW of Al-TRIP steel, similar chemistry as AT steel in the present study, which was a remainder of high temperature δ-ferrite that did not fully transform to austenite during cooling. It is interesting to note that in the present study fusion zone in RSW of AT steel formed lower fraction of δ-ferrite (15 ± 3%) than in LBW (30%) [14]. This difference is attributed to higher cooling rate in RSW which suppress the formation of δ-ferrite by stabilizing non-equilibrium austenite which on further cooling transforms to martensite phase [35]. So, it was concluded that in the AT fusion zone δ-ferrite was stabilized due to sufficient Al-content (>1.05 wt.%). In addition to ferrite stabilization, Al also facilitates the formation of bainite by accelerating the bainitic transformation kinetics due to higher nucleation rate [2,29]. Thus, microstructure of the Al-containing fusion zone (AT and AST) in the present study contained bainitic regions (Figs. 4a and 7a–c).

3.4. Fusion zone hardness of the TRIP steel welds

The comparison of the hardness profiles measured from the center of the fusion zone across the weldment for the TRIP steels studied is plotted in Fig. 9. It is to be noted that for AST weld no significant variation in the fusion zone hardness on AT side (460–495 HV) and ST side (485–510 HV) was seen, thus, only the hardness profile on the AT side of the weld is shown in Fig. 9. The average fusion zone hardness in RSW of the TRIP steels studied is compared in Table 4. It was clearly seen that the fusion zone in ST steel has higher hardness (526 ± 10 HV) compared to that in AT steel (425 ± 22 HV); whereas AST fusion zone has hardness in between the ST and AT steel i.e. 486 ± 15HV (Table 4). Lower hardness in the AT fusion zone was mainly attributed to its

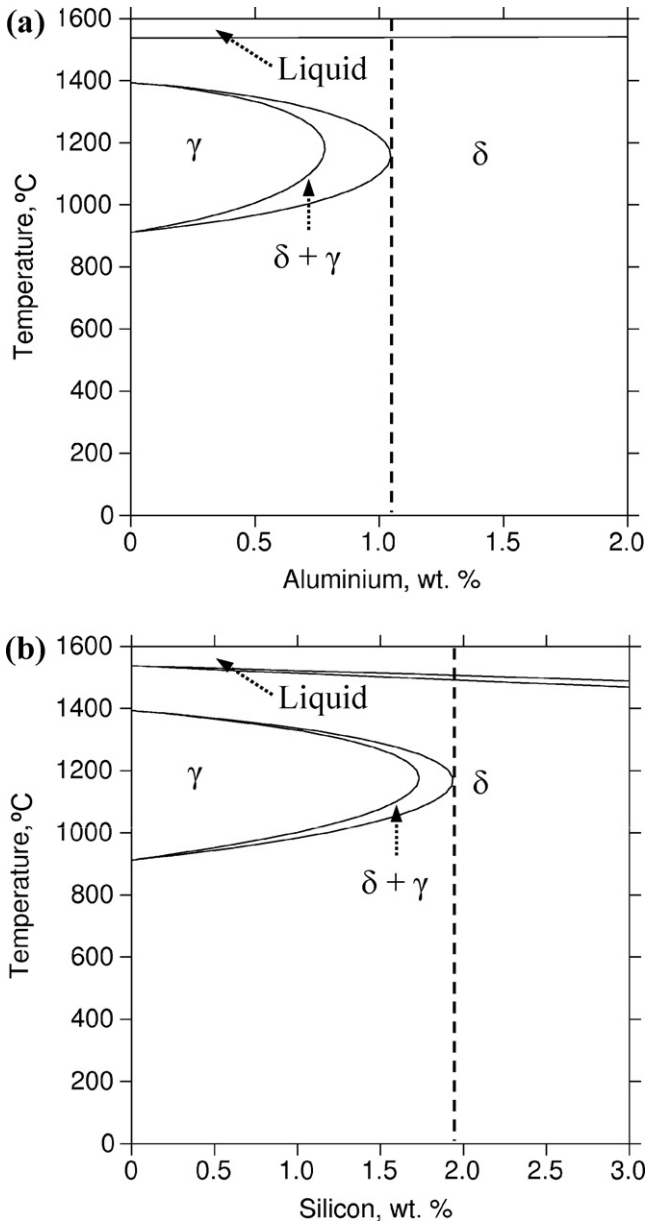

Fig. 8. Fe-rich side of binary (a) Fe–Al and (b) Fe–Si phase diagram illustrating that δ-ferrite phase is stabilized in steel if Al or Si content exceeds 1.05 wt.% or 1.95 wt.%, respectively.

microstructure containing soft ferrite phase (Figs. 3a and 4a) and possibly to lower solid solution hardening by Al compared to Si [36]. Furthermore, with reference to fusion zone microstructure (Figs. 3b, 5 and 7) and the resultant not significant variation in fusion zone hardness (Fig. 9), it was confirmed that homogeneous composition was achieved within the AST weld nugget. It is well known that hardness is an indication of the strength of spot-welded joints. In general, increase in hardness results in increase in

Table 4
Comparison of average fusion zone hardness (HV) of the spot welded TRIP steels studied with that of the fusion zone in LBW of TRIP steels with similar chemistries [14]. It is to be noted that LBW article has not reported fusion zone of AST steel.

Steel	RSW	LBW
AT	425 ± 22	331 ± 4
AST	486 ± 15	–
ST	526 ± 10	484 ± 5

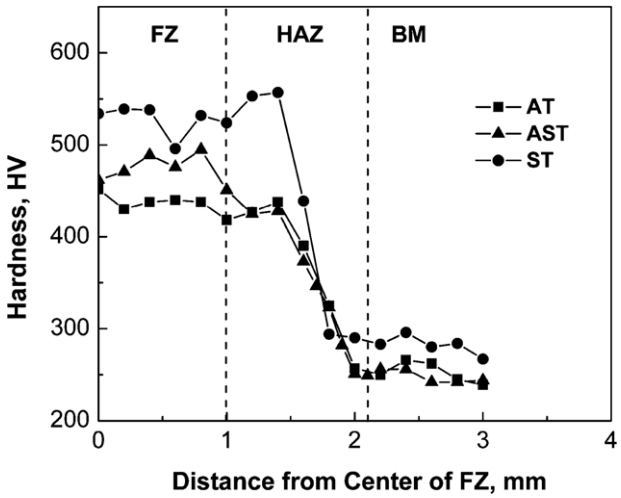

Fig. 9. Hardness profiles of the weldments in all the TRIP steels studied; where FZ: fusion zone, HAZ: heat affected zone, and BM: base metal.

strength whereas decreasing formability or ductility. The hardness of the ST steel fusion zone is appreciably higher as a consequence of the single phase microstructure comprising lathy martensite (Figs. 3c and 4b) in comparison to the AT steel fusion zone which contains mixed microstructure containing softer phases like ferrite and bainite along with martensite (Figs. 3a and 4a); this results is in good agreement with the earlier reports [17,36–38].

To analyze the effect of cooling rate on fusion zone hardness, results of TRIP steels with similar chemistries welded in LBW reported by Xia et al. [14] are also enlisted in Table 4. It is seen that the fusion zone hardness increased from AT to ST steel which implies decrease in Al content or increase in Si content in the fusion zone (Table 1). The hardness change with Al and Si content was promptly correlated to the corresponding microstructure. For example, AT steel (1.27Al–0.08Si) forming soft ferrite phase in the fusion zone (Figs. 3a and 4a) leads to lower hardness and ST steel (0.03Al–1.62Si) containing fully martensitic microstructure (Figs. 3c and 4b) had higher hardness; whereas AST steel has Al and Si content (Table 1) lying in between AT and ST steel thus indicated hardness in between the respective fusion zone as confirmed by the mixed microstructure containing martensite and bainite phase (Figs. 3b, 5, and 7). Furthermore, it was also seen that RSW resulted in higher fusion zone hardness overall which is attributed to the very high cooling rate in RSW (>3000 K/s) as can be estimated from Fig. 2, compared to moderate cooling rate of 53 K/s in LBW [15,38] which facilitates formation of different microstructural constituents in the fusion zone. For instance, if we compare AT fusion zone higher hardness was observed in RSW due to formation of lower fraction ($15 \pm 3\%$) of soft ferrite phase (Fig. 3a) compared to LBW (30%) [14]. However, as no other phase was found in ST fusion zone in both RSW and LBW [14] apart from martensite structure and the carbon content in the steel was same, it was concluded that RSW of ST steel resulted in finer grains/packets of martensite phase due to faster cooling leading to the higher hardness compared to LBW.

4. Conclusions

Fusion zones of TRIP steels in resistance spot welding were characterized, with respect to fusion zone microstructure and hardness, and compared with the results of laser welding of similar steels. Following conclusions were drawn from the study:

1. Fusion zone microstructure was dependent on its chemistry: (i) AT steel formed mixture of ferrite (15%) along with bainite and martensite, (ii) AST fusion zone contained mostly martensite with few regions of upper and lower bainite (20%) accompanied by occasional martensite twins, (iii) whereas ST fusion zone contains single phase martensite structure.
2. Martensite phase observed was lath structure with stabilization of interlath austenite; the fraction of which was observed to increase with increase in Si-content in the fusion zone.
3. An increase in average fusion zone hardness with decrease in Al content or increase in Si-content was observed; which was attributed to increasing fraction of hard martensite phase and decrease in soft ferrite fraction in the microstructure. Accordingly, hardness of the fusion zone followed the trend: AT (425 ± 22 HV) → AST steel (486 ± 15 HV) → ST steel (526 ± 10 HV).
4. Effect of cooling rate on the hardness of the fusion zone suggested that higher cooling rate (>3000 K/s) in RSW leads to higher hardness compared to LBW with moderate cooling rate (53 K/s), irrespective of the steel chemistry, due to decrease in softer ferrite phase (AT steel) in the microstructure or refinement of martensite grains/packets (ST steel).

Acknowledgments

The authors would like to acknowledge the financial support from Auto21, one of the Networks of Centres for Excellence supported by the Government of Canada, The Initiative for Automotive Manufacturing Innovation (IAMI) supported by the Ontario Government, ArcelorMittal Dofasco Inc., Hamilton, Canada. Authors are thankful to Prof. S. Haro Rodriguez for his help in carrying out the XRD study at MPyM-EPMM Academic Unit of Engineering, Autonomous University of Zacatecas, Mexico.

References

[1] H. Bhadeshia, R. Honeycombe, Steels: Microstructure and Properties, third ed., Butterworth-Heinemann, Oxford, UK, 2006.
[2] B.C. De Cooman, Curr. Opin. Solid State Mater. Sci. 8 (2004) 285.
[3] V.F. Zackay, E.R. Parker, R. Busch, Trans. ASM 60 (1967) 252.
[4] S. Zaefferer, J. Ohlert, W. Bleck, Acta Mater. 52 (2004) 2765.
[5] P.J. Jacques, Curr. Opin. Solid State Mater. Sci. 8 (2004) 259.
[6] H.K.D.H. Bhadesia, ISIJ Int. 42 (2002) 1059.
[7] J. Maki, J. Mahieu, B.C. De Cooman, Proc. 5th Int. Conf. on Zinc and Zinc Alloy Coated Steel Sheet (Galvatech 2001), Centre de Researches Meâtallurgiques, Bruxelles, Belgium, 2001.
[8] E. Giraulta, A. Mertensb, P. Jacquesb, Y. Houbaertc, B. Verlindena, J.V. Humbeecka, Scr. Mater. 44 (2001) 885.
[9] P.J. Jacques, E. Girault, P. Harlet, F. Delannay, ISIJ Int. 41 (2001) 1061.
[10] Committee on Automotive Applications, AHSS – Application Guidelines, International Iron and Steel Institute, Washington, DC, 2006.
[11] V.H. Baltazar Hernandez, M.L. Kuntz, M.I. Khan, Y. Zhou, Sci. Technol. Weld. Joining 13 (2008) 769.
[12] S. Daneshpour, S. Riekehr, M. Kocak, V. Ventzke, A.I. Koruk, Sci. Technol. Weld. Joining 12 (2007) 508.
[13] T.K. Han, S.S. Park, K.H. Kim, C.Y. Kang, I.S. Woo, J.B. Lee, ISIJ Int. 45 (2005) 60.
[14] M. Xia, Z. Tian, L. Zhao, Y.N. Zhou, ISIJ Int. 48 (2008) 483.
[15] J. Chen, K. Sand, M.S. Xia, C. Ophus, R. Mohammadi, M.L. Kuntz, Y. Zhou, D. Mitlin, Metall. Mater. Trans. A 39A (2008) 593.
[16] M. Xia, Z. Tian, L. Zhao, Y.N. Zhou, Mater. Trans. JIM 49 (2008) 746.
[17] M.I. Khan, L.M. Kuntz, Y. Zhou, Sci. Technol. Weld. Joining 13 (2008) 294.
[18] M. Amrithalingam, M. Hermans, I. Richardson, Metall. Mater. Trans. A 40A (2009) 901.
[19] C. Ma, D.L. Chen, S.D. Bhole, G. Boudreau, A. Lee, E. Biro, Mater. Sci. Eng. A 485 (2008) 334.
[20] H. Ghazanfari, M. Naderi, M. Iranmanesh, M. Seydi, A. Poshteban, Mater. Sci. Eng. A 534 (2012) 90.
[21] X. Liao, X. Wang, Z. Guo, M. Wang, Y. Wu, Y. Rong, Mater. Character. 61 (2010) 341.
[22] S. Brauser, L.A. Pepke, G. Weber, M. Rethmeier, Mater. Sci. Eng. A 527 (2010) 7099.
[23] C. Liu, Z. Zhao, D.O. Northwood, Y. Liu, J. Mater. Process. Technol. 113 (2001) 556.

[24] Resistance Welding Manufacturing Alliance (RWMA), /(accessed on 10.11.2011).
[25] ANSI/AWS/SAE D8.9-97, Recommended Practices for Test Methods for Evaluating the Resistance Spot Welding Behavior of Automotive Sheet Steels Materials, American Welding Society, Miami, 1997.
[26] B.L. Bramfitt, A.O. Benscoter, Metallographer's Guide: Practices and Procedures for Irons and Steels, first ed., ASM International, 2002.
[27] http://www.rccm.co.jp/seihin/quickspot/index.html (accessed on 13.11.2011).
[28] V.H. Baltazar Hernandez, Y. Okita, Y. Zhou, Weld. J., in press.
[29] C. Garcia-Mateo, F.G. Caballero, H.K.D.H. Bhadesia, ISIJ Int. 43 (2003) 1821.
[30] J.E. Gould, S.P. Khurana, T. Li, Weld. J. 85 (2006) 111s.
[31] B.V. Narashima Rao, Metall. Trans. A 10A (1979) 645.
[32] H.K.D.H. Bhadesia, Bainite in Steels, second ed., The Institute of Materials, London, 2001.
[33] S.J. Kim, C.G. Lee, I. Choi, S. Lee, Metall. Mater. Trans. A 32A (2001) 505.
[34] O. Akelsen, O. Grong, J. Solberg, Mater. Sci. Technol. 3 (1987) 649.
[35] S.S. Babu, J.W. Elmer, S.A. David, M.A. Quitana, Proc. R. Soc. (London) 458 (2002) 811.
[36] P.A. Manohar, K. Kunishige, T. Chandra, M. Ferry, Mater. Sci. Technol. 118 (2002) 856.
[37] P.J. Jacques, E. Girault, A. Mertens, B. Verlinden, J. Van Humbeeck, F. Delannay, ISIJ Int. 41 (2001) 1068.
[38] M. Pouranvari, H.R. Asgari, S.M. Mosavizadch, P.H. Marashi, M. Goodarzi, Sci. Technol. Weld. Joining 12 (2007) 217.